Published in final edited form as:
Nature. ; 483(7390): 494–497. doi:10.1038/nature10881.

Identification and characterization of a bacterial hydrosulfide ion channel

Bryan K. Czyzewski[1,2] and **Da-Neng Wang**[1,3,*]

[1]The Helen L. and Martin S. Kimmel Center for Biology and Medicine at the Skirball Institute of Biomolecular Medicine, New York University School of Medicine, 540 First Avenue, New York, NY 10016, USA

[2]Molecular Biophysics Graduate Program, New York University School of Medicine, 540 First Avenue, New York, NY 10016, USA

[3]Department of Cell Biology, New York University School of Medicine, 540 First Avenue, New York, NY 10016, USA

Abstract

Believed to have been critical to the origin of life on Earth [1], the hydrosulfide ion (HS^-) and its undissociated form, hydrogen sulfide (H_2S), continue to play a prominent role in physiology and cellular signaling [2]. As a major metabolite in anaerobic bacterial growth, hydrogen sulfide is a product of both assimilatory and dissimilatory sulfate reduction [2–4]. These pathways can reduce various oxidized sulfur compounds including sulfate, sulfite and thiosulfate. The dissimilatory sulfate reduction pathway uses this molecule as the terminal electron acceptor for anaerobic respiration, where it produces excess amounts of H_2S[4]. The reduction of sulfite is a key intermediate step in all sulfate reduction pathways. In *Clostridium* and *Salmonella*, an inducible sulfite reductase is directly linked to the regeneration of NAD^+, which has been suggested to play a role in energy production and growth, as well as in the detoxification of sulfite [3]. Above a certain concentration threshold, both H_2S and HS^- nhibit cell growth by binding the metal centers of enzymes and cytochrome oxidase[5], necessitating a release mechanism for the export of this toxic metabolite from the cell [5–9]. Through a combination of genetic, biochemical and functional approaches, we have identified a hydrosulfide ion channel (HSC) in the pathogen *Clostridium difficile*. The HS^- channel is a member of the formate-nitrite-transport (FNT) family, in which ~50 HSC genes form a third subfamily alongside those for formate (FocA) [10,11] and for nitrite (NirC) [12]. In addition to HS^- ions, HSC is also permeable to formate and nitrite. Such polyspecificity can be explained by the conserved ion selectivity filter observed in the HSC crystal structure. The channel has a low open probability and is tightly regulated, to avoid decoupling of the membrane proton gradient.

*Correspondence and requests for materials should be addressed to D.N.W. (wang@saturn.med.nyu.edu).

Supplementary Information is linked to the online version of the paper at www.nature.com/nature.

Author Contributions: B.K.C did the experiments. B.K.C. and D.N.W. wrote the manuscript.

The atomic coordinates and structure factors for high-, medium- and low-pH have been deposited under access codes 3TDO, 3TDR and 3TDP, respectively, and those of the K16S, L82V, T84A, K148E and F194I mutants under the codes 3TE2, 3TDX, 3TE1, 3TE0and 3TDS, respectively.

The authors declare no competing financial interests. Readers are welcome to comment on the online version of this article at www.nature.com/nature.

The authors dedicate this work to the memory of Lennart Philipson.

As a weak acid with a pK_a of 6.8 and a second pK_a of 19, over 80 percent of the H_2S in a biological system will exist in its ionized form as HS^- [2,13]. To account for membrane permeation of intracellularly produced hydrogen sulfide [6,9], a channel for HS^- or H_2S has been suggested [5,7], with the water channel aquaporins (AQPs) as possible candidates [8]. While studies in planar lipid bilayers indicate that the aquaporin from *Archaeoglobus fulgidus* is not permeable to H_2S and that the lipid bilayer provides little resistance to H_2S permeation [9], in the ventworm *Riftia pachyptila* it has been shown that HS^- ions, but not H_2S, are selectively transported through its outer epithelium into its vasculature[5].

Despite its high permeability across the lipid bilayer, we argue that the weak acidity of H_2S necessitates a release mechanism for its ionized form, HS^- (Fig. 1a). As a weak acid with a pK_a of 6.8, H_2S can diffuse readily across the lipid bilayer. Therefore, the distribution of H_2S and HS^- on both sides of the cell membrane is directly proportional to the pH differential as described by the Henderson-Hasselbalch equation [14]. Since cellular pH is kept at neutral levels, and extracellular pH is typically one to two units more acidic, at equilibrium the HS^- concentration will be 10–100 fold greater on the inside of the cell in the absence of a release mechanism for the HS^- anions. Therefore, given its significant toxicity, it would be beneficial to directly expel this ion across the membrane by the quickest mechanism available—an ion channel.

Recently, a novel family of anion channels for short-chain acids has been functionally characterized [11,15,16]. Members of the FNT family transport various anions during anaerobic bacterial growth [10,12,17]. Based on sequence homology, however, only about half of its two thousand identified members clearly belong to either the FocA or NirC subfamily (Figs. 1b&c, Supplementary Figs. 1&2). Intriguingly, for both FocA and NirC, each channel gene is genetically linked to its reductase partner: *FocA* to the formate reductase *pflB* [10] and *NirC* to the nitrate reductase *NirBD* [12] (Fig. 1b). Our phylogenetic analysis of bacterial genes suggests the existence of additional channel subfamilies in the FNT family (Fig. 1c, Supplementary Fig. 1). One such subfamily is a group of ~50 homologous genes, temporarily termed FNT3, found in various species of *Clostridium*, major human pathogens grown under strictly anaerobic conditions. As it is linked with a reductase gene, the *asrABC* operon [18] (Fig. 1b), we hypothesized that *FNT3* might encode a channel for HS^- or related ions. AsrABC reduces sulfite (SO_3^{-2}) into sulfide (S^{-2}), which becomes instantly converted into H_2S and HS^- under physiological conditions.

asrABC from *Salmonella* is the only such operon that has been characterized thus far. Its overexpression in *E. coli,* which lacks this biochemical pathway, was previously shown to reduce SO_3^{-2} to H_2S [19]. To first verify whether the homologous *asrABC* operon from *C. difficile* also encodes an SO_3^{-2} reductase, we tested the growth of *E. coli* transformed with the *C. difficile asrABC* genes, plated on bismuth sulfite agar [19,20]. When *C. difficile asrABC* was induced, *E. coli* were able to overcome the expected growth inhibition by reducing SO_3^{-2} to H_2S (Fig. 1d, Supplementary Fig. 3). Darkening along the edges of the colonies, formed by bismuth/iron sulfide precipitation, further indicated that H_2S gas was being produced. This showed that the *asrABC* genes from *C. difficile* do indeed encode for an SO_3^{-2} reductase, which in turn supports the notion that the *FNT3* gene in the *asrABC* operon may indeed encode a channel for SO_3^{-2}, or its reduced product, HS^-.

To determine whether the FNT3 protein from *C. difficile* functions as a channel for HS^- or SO_3^{-2}, we then carried out whole cell transport, ion – protein binding in solution and transport-inhibition assays in reconstituted proteoliposomes. First, we transformed sulfide-producing *S. typhimurium*, which lacks an HS^- channel, with the *C. difficile FNT3* gene. In SO_3^{-2} supplemented minimal medium, the *FNT3*-expressing *S. typhimurium* released a high level of HS^- ions into the culture medium (Fig. 2a, Supplementary Fig. 4). This increase in

extracellular HS^- was specific for HS^- produced by the endogenous cytoplasmic AsrABC; when the other sulfide-producing reductase in the cell, the periplasmic thiosulfate reductase, was engaged with its substrate thiosulfate, little effect on the extracellular concentration of HS^- was observed. This indicates that the measured HS^- was generated by SO_3^{-2} reduction by the cytoplasmic AsrABC and then exported. Such an FNT3-linked increase in HS^- production in *S. typhimurium* can be attributed to either increased import of SO_3^{-2} or increased HS^--export from the cell. It follows that FNT3 could be an ion channel for SO_3^{-2} or HS^-.

An ion channel protein is often stabilized by its permeating ions through their direct interaction with its selectivity filter [21]. Therefore, we tested whether purified FNT3 protein interacts with the monovalent HS^- or the divalent SO_3^{-2}. Using size-exclusion chromatography of purified protein samples incubated at elevated temperatures, we found that at pH 8.0 the presence of HS^- ions was able to increase the nominal melting temperature of the FNT3 protein by 8 °C, whereas SO_3^{-2} had little effect (Fig. 2b, Supplementary Table 1). This result is consistent with the hypothesis that FNT3 functions as an HS^- channel but is probably impermeable to SO_3^{-2}. Intriguingly, three other monovalent anions, formate, nitrite and chloride, also increased the melting temperature of the FNT3 protein, but to a lesser degree (3 – 4 °C).

We went on to identify the permeable ion(s) of the FNT3 protein *in vitro*. As channels in the FNT family are expected to have slow conductance rates [11], we measured FNT3 transport activity using a concentrative uptake assay [11,22]. Given that HS^- ions at concentrations needed to set up a sufficient electrochemical gradient (~150 mM) are severely disruptive to the membrane, we chose to measure the permeability of FNT3 using another interacting ion (Fig. 2b), formate. Proteoliposomes reconstituted at pH 8.0 from purified *C. difficile* FNT3 protein were found to be permeable to formate, although at a lower rate than FocA from *Vibrio cholerae* (Fig. 2c). This permeability to formate by FNT3 allowed us to search for other ions that directly compete with formate for transport. Indeed, when HS^- or nitrite was present in the buffer outside the proteoliposomes, the uptake of formate was dramatically inhibited (Fig. 2d). In the physiological range of 1—2 mM sulfide, ~70% inhibition was observed, while at the highest concentration tested (15 mM), HS^- and nitrite inhibited the uptake of formate by 90% and 70%, respectively.

Such direct competitive inhibition (Fig. 2c), coupled with whole cell transport assays (Fig. 2a) and *in vitro* binding assays (Fig. 2b), collectively indicates that the FNT3 protein from *C. difficile* is likely to be a channel for the hydrosulfide ion, HS^-. Although the channel is also permeable to formate and nitrite ions, the *FNT3* gene is directly linked to the *asrABC* sulfite reductase operon (Fig. 1b); we have therefore tentatively named this protein a hydrosulfide ion channel (HSC). A definite understanding of the physiological role of these channels will need to be confirmed by *in vivo* experiments such as genetic deletion studies.

To understand the transport mechanism of the HSC/FNT3 channel from *C. difficile* (Supplementary Fig. 5), we determined its crystal structure at high-pH (pH = 9.0) to 2.2 Å resolution (Fig. 3a, Supplementary Table 2). The HSC protein adopts the AQP/FocA fold [11,23], and forms a pentamer like FocA, with the five protomers having identical structure (Supplementary Figs. 6–8). The twofold inverted symmetry between the first and second half of the protein goes beyond that observed in FocA and extends to the pore-lining helices TM2b and TM5b (Supplementary Fig. 8b), two salt bridge triads on the periplasmic and the cytoplasmic side (Lys148-Glu200-Asn205 and Lys16-Glu81-Asn86) (Figs. 4a–c) and the two short helices parallel to the membrane (helix P on the periplasmic surface and helix N at the N-terminus on the cytoplasmic surface) (Supplementary Fig. 8b). This helix

N, via the Lys16-Glu81-Asn86 salt bridge triad, buttresses TM2b and TM5a, making the cytoplasmic side of the protein more closed and rigid than that in FocA [11].

The pore for ion permeation, located at the center of each protomer, contains the selectivity filter formed by a cytoplasmic slit and a periplasmic ring in the middle of the membrane (Figs. 3a&b). The radius of the cytoplasmic slit measures 0.8 Å which is too small for an HS^- ion (radius 1.7 Å [24]) to pass through (Supplementary Figs. 9–11). Therefore, the HSC channel in the crystal structure is probably in a closed state. As expected from the sequence conservation in the selectivity filter with that of FocA (Supplementary Fig. 2), the positions or orientations of key residues changed only slightly in HSC (Supplementary Fig. 10). Such conservation explains the permeability of HSC to HS^-, as well as to formate and nitrite. When a residue at the cytoplasmic slit or the periplasmic ring is mutated into a smaller residue—Leu82->Val or Phe194->Ile—the pore size is widened, as shown in the crystal structures of the mutant protein (Fig. 3b, Supplementary Table 2), and the formate transport rate of the channel is significantly increased (Fig. 3d). Interestingly, in the crystal structure of the Leu82Val mutant, electron density was observed in the cytoplasmic slit (Fig. 3c). This density, heavier than a water molecule—judged by a B-factor fourfold lower than the surrounding atoms—could be accounted for by a Cl^- or an HS^- ion. Due to their similar sizes and chemical properties, it has been previously observed that Cl^- and HS^- ions often bind to the same site in protein crystal structures [25].

The observed polyspecificity of HSC is typical for anion channels [26–28], most likely shared by the FocA and NirC channels as well. Such polyspecific anion recognition is at least partially due to the diffused nature of the electron cloud of anions [29], in contrast to the point-like charge properties of cations. In the meantime, each type of HSC channel in this ancient protein family, coupled with its specific metabolic pathway, is expected to have its own preference for permeating ions, and that preference is probably due to the small structural variations in the selectivity filter that we observed here (Supplementary Fig. 10).

The expulsion of toxic levels of HS^- from the cytoplasm through HSC needs to be balanced against the potential risk of the uncoupling of the membrane proton gradient. Freely diffusible H_2S and other weak, short-chain acids will dissociate into an anion and a proton in the cytoplasm (Fig. 1a). As the anion is expelled, there will be an intracellular net accumulation of protons. Therefore, the ground state of HSC is likely to be closed and its opening tightly regulated.

Indeed, the HSC structure we determined at high pH is in its closed state (Fig. 3, Supplementary Figs. 9–11). We then asked the question, how easily could this channel be opened? As the homologous FocA channel can be opened by pH or cytoplasmic formate concentration [11,16], we first investigated possible pH-dependent structural changes of HSC by determining its crystal structure at pH 7.5 (3.2 Å resolution) and at pH 4.5 (3.0 Å) (Supplementary Table 2). The protein structures obtained at these neutral and low pHs were the same as the 2.2 Å structure at pH 9.0 (Supplementary Fig. 12), and the channel remained closed. We then studied the two salt bridge triads, both of which contain a glutamate residue that could potentially function as a pH sensor (Fig. 4a–c). When either of the salt bridges was broken, by mutating Lys16->Ser or Lys148->Glu, the HSC crystal structure did not change and the channel still remained closed (Supplementary Fig. 13, Supplementary Table 2). Consistent with these structural results, their transport rate did not increase (Fig. 4d).

To determine whether HSC is gated by anion concentration in a similar manner as the *V. Cholerae* FocA [11], in which the competition of formate with Thr90 from the Ω loop for hydrogen bonding to His208 in the selectivity filter opens the channel, we mutated the equivalent threonine in HSC, Thr84, to an alanine and determined its 2.4 Å crystal structure

(Supplementary Table 2). This mutant structure did not differ from the closed wild-type channel, and no increase in transport was detected (Fig. 4d & Supplementary Fig. 14). As Thr84, Lys16 and Lys148 all line the ion permeation pathway, mutation of these residues slightly reduced the ion permeation rate of the channel. Therefore, we conclude that the opening of HSC is indeed tightly regulated and the channel has a much lower open probability than FocA [11,16].

The low open probability of HSC observed here is consistent with its physiological role in the cell. The opening of HSC probably requires significant movement of helix 2b. As helix 2b is "held" in space by the cytoplasmic helix N (Fig. 4a), the movement of the latter, for example, by direct interaction with a cytoplasmic enzyme in the same metabolic pathway, can trigger the opening of the channel. Of course, we have no evidence for such a hypothesis, and its validation can only be achieved by further experimentation, which we expect would reveal greater variations in both the gating mechanism and anionic preference of FNT channels.

METHODS

Phylogenetic analysis

Phylogenetic data for 474 bacterial and archaeal members of the Formate-Nitrite Transport family were obtained from the HOGENOM database [30], aligned with program Jalview [31] and plotted with program Archaeopteryx [32]. Genomic sequences and operon annotations were derived from the NCBI Genbank nucleotide database [33].

Bismuth sulfite Agar plate assay

The *FNT3/HSC* gene was isolated from *Clostridium difficile* strain 630. The genes for *Clostridium difficile asrA* (NCBI ID: 4915353) and *asrB* (ID: 4915352) were cloned into pCDFDuet-1 (EMD Biosciences) and the genes for *C. difficile asrC* (ID: 4915351) and *HSC* (ID: 4915350) were cloned into pACYCDuet-1 (EMD Biosciences). Bismuth sulfite agar plates [20] were freshly prepared following the manufacturer's protocol and supplemented with 1 mM Isopropyl β-D-1-thiogalactopyranoside and antibiotics chloramphenical and spectinomycin. *E. coli* BL21 (DE3) cells were transformed with the indicated vectors and streaked, and colonies were allowed to grow at 37 °C for 48 hours. The bismuth sulfite agar [20] contained the ATP-synthase-inhibitor brilliant green [19] and high concentrations of SO_3^{-2}. When *C. difficile asrABC* was induced, *E. coli* were able to overcome the growth inhibition by producing ATP via glycolysis by reducing SO_3^{-2} to H_2S.

Whole cell *in vivo* transport assay

Salmonella typhimurium LT2 was transformed with the HSC gene cloned into a pBAD vector (Invitrogen). Cells were adapted in MOPS medium supplemented with 10 mM glucose and thiamine at 1 μg/ml. A fraction of each culture (5 ml) was centrifuged and resuspended in fresh media supplemented with ampicillin, 0.2% arabinose and either 6 mM sodium sulfite or 6 mM sodium thiosulfate. Aliquots were incubated at 37°C for 6 hours and then centrifuged to pellet bacteria. Media was gently poured into an equal volume of sulfide antioxidant buffer. Exported sulfide was measured using a combination silver-sulfide electrode (Cole-Palmer). The concentration of sulfide in the medium was determined using standards of known sodium sulfide concentrations in the same antioxidant buffer.

Protein purification

The gene encoding HSC was cloned into a modified pBAD vector (Invitrogen) creating a C-terminal TEV-Flag-10xHis fusion protein and transformed into *E. coli* BL21 *plysS* (Sigma-Aldrich) cells [11,34,35]. Transformed cells were grown at 37 oC to an OD_{600} of 1.0 and

induced with 0.2 % of arabinose for 4 hours. Cells were collected and lysed by passing twice through an Emulsiflex cell disrupter (Avestin). Lysate was clarified by a low speed spin at 12,000 × g and solubilized with 1% β-dodecyl-maltopyranoside (DDM, Anatrace). Solubilized lysate was incubated with Ni^{+2} –NTA resin (Qiagen) and the bound protein was eluted with buffer containing 1.1% β-octyl-glucopyranoside (OG, Anatrace), 50 mM Tris 8.0, 200 mM NaCl, 300 mM imidazole and 10% glycerol. The protein sample was incubated with TEV protease overnight to remove the tags, followed by size exclusion chromatography in Superdex 200 in 25 mM TRIS, pH 6.8, 100 mM NaCl and 1.1% OG.

Mass Spectrometry

The mass of purified HSC protein was determined using matrix-assisted laser desorption/ ionization time-of-flight (MALDI-TOF) mass spectrometry in the laboratory of Dr. T. Neubert following published protocols [36–38].

Protein-ion interaction assay

Ion-binding-induced thermostability of purified protein samples was measured using size exclusion chromatography. Aliquots of 100 mg of Ni^{+2} –NTA purified protein were incubated for 10 minutes in a thermocycler at increasing temperatures. Samples were injected onto a Shodex KW804 analytical size exclusion chromatography column (Thomson, Clear Brook, VA) on HPLC (Shimadzu, Columbia, MA) equilibrated in 200 mM Na_2SO_4, 50 mM Tris pH 8.0, 3 mM NaN_3 and 0.05 % DDM. The height of monodisperse peak was used to quantify the amount of remaining sample. The nominal melting temperature T_m, defined as the temperature at which 50% of the protein remained soluble, was calculated by fitting the data to a Boltzmann sigmoidal model in Prism5 (GraphPad Software, La Jolla, CA). For screening of various compounds, 20 mM of each sodium salt was added prior to incubation.

Proteoliposome reconstitution and *in vitro* transport assay

Transport of radiolabeled formate was measured in a concentrative uptake assay [11,22]. *E. coli* total lipids were aliquoted in chloroform and dried under nitrogen. Following resuspension in intraliposomal buffer (150 mM sodium formate and 50 mM Tris pH 8.0), lipids were overlayed with nitrogen, freeze thawed 10 times, vortexed and sonicated to homogeneity. Proteoliposomes were formed by the addition of 1% OG and Ni^{+2} –NTA purified HSC at a protein to lipid ratio of 1:10,000 (w/w). OG detergent was removed by incubation with $400 \cdot mg \cdot ml^{-1}$ Bio-Beads SM2 (Bio-Rad) overnight. Proteoliposomes were then subjected to extrusion through 400-nm membrane filter and then frozen at −20 °C until use. Concentrated reuptake of formate was initiated by buffer exchanging 200 ml of thawed proteoliposomes over 2 ml of G50 Sephadex swollen in extraliposomal buffer (150 mM glutamate, 50 mM Tris pH 8.0). 450 μM ^{14}Clabeled sodium formate (American Radiolabeled Chemical) was added to the collected proteoliposomes, and the assays were terminated by centrifuging a 20 ml sample at 1000 × g for 1 minute at each time point through a G-50 Probequant™ Micro-column (GE Healthcare) to remove the external radiolabeled formate.

The amount of transported radiolabeled formate was quantified by adding 1 ml of scintillation fluid to each sample and emitted photons were counted using a Wallac scintillation counter. For competition assays, increasing concentrations of sodium sulfite, sodium nitrite or sodium hydrosulfide at 0, 0.15, 0.6, 3 and 15 mM, were added prior to the addition of radiolabeled formate.

Protein crystallization

High pH, primitive orthorhombic crystals of HSC were grown using the vapor diffusion method, by mixing protein at a concentration of 11 mg/ml in a 1:1 ratio with reservoir solution containing 25–27% (v/v) PEG 400, 100 mM Tris pH 7.0–9.0, 100 mM sodium sulfite, with or without 50 mM sodium hydrosulfide. Medium pH, monoclinic crystals were grown in reservoir substituted with 100 mM sodium nitrite, pH 7.5. Low pH, C-centered orthorhombic crystals were grown in buffer containing 100 mM sodium sulfite, 100 mM sodium nitrite, 8–10% (w/v) PEG 6000, 100 mM zinc acetate and 100 mM sodium acetate pH 4.5.

Structure determination

X-ray diffraction data were collected at beamlines X25 and X29 in the National Synchrotron Light Source of the Brookhaven National Laboratory and 23-ID in the Advanced Photon Source of Argonne National Laboratory. Images were processed and scaled using the HKL2000 suite [39]. The structure was solved by molecular replacement using the *V. cholerae* FocA structure (PDB code 3KLY) [11] as a search model. Models were built using Phenix Autobuild [40] and manually adjusted using COOT [41]. Refinement was carried out using Phenix Refine [40]. Pore size of the channel was calculated using HOLE [42], and structure figures were generated using the program PYMOL [43]

Supplementary Material

Refer to Web version on PubMed Central for supplementary material.

Acknowledgments

We are grateful the staff at beamlines X25 and X29 of the National Synchrotron Light Source in the Brookhaven National Laboratory and at the 23ID at the Advanced Photon Source at the Argonne National Laboratory for assistance in X-ray diffraction experiments. We thank A.B, Waight for suggesting the project, J.J. Marden for assistance with cloning of mutants, T. Neubert and S. Blais for mass spectrometry measurements, the 2010 CCP4 Workshop for assistance in processing diffraction data, and A. David, H. Jackson, N.K. Karpowich, J.J. Marden, R.L. Mancusso, Y. Pan and M. Zhou for helpful discussions. This work was financially supported by the NIH (R01-GM093825, R01-DK073973, R01-MH083840 and U54-GM075026). B.K.C. was partially supported by an NIH Supplement Grant to Promote Diversity in Health-Related Research (R01-DK053973-08A1S1) and an NIH predoctoral fellowship (F31-AI086072).

References

1. Wachtershauser G. Groundworks for an evolutionary biochemistry: the iron-sulphur world. Prog Biophys Mol Biol. 1992; 58:85–201. [PubMed: 1509092]
2. Kabil O, Banerjee R. Redox biochemistry of hydrogen sulfide. J Biol Chem. 2010; 285:21903–21907. [PubMed: 20448039]
3. Dhillon A, Goswami S, Riley M, Teske A, Sogin M. Domain evolution and functional diversification of sulfite reductases. Astrobiology. 2005; 5:18–29. [PubMed: 15711167]
4. Rabus, R.; Hansen, T.; Widdel, F. Dissimilatory sulfate- and sulfur-reducing prokaryotes. In: Dworkin, M., et al., editors. The Prokaryotes: Ecophysiology and Biochemistry. Vol. 2. Springer; Heidelberg: 2006. p. 659-768.
5. Goffredi SK, Childress JJ, Desaulniers NT, Lallier FJ. Sulfide acquisition by the vent worm *Riftia pachyptila* appears to be via uptake of HS^-, rather than H2S. J Exp Biol. 1997; 200:2609–2616. [PubMed: 9359367]
6. Jacques AG. The kinetics of penetration: Xii. Hydrogen sulfide. J Gen Physiol. 1936; 19:397–418. [PubMed: 19872936]
7. Freytag JK, et al. A paradox resolved: sulfide acquisition by roots of seep tubeworms sustains net chemoautotrophy. Proc Natl Acad Sci U S A. 2001; 98:13408–13413. [PubMed: 11687647]

8. Lee JK, et al. Structural basis for conductance by the archaeal aquaporin AqpM at 1.68 Å. Proc Natl Acad Sci U S A. 2005; 102:18932–18937. [PubMed: 16361443]
9. Mathai JC, et al. No facilitator required for membrane transport of hydrogen sulfide. Proc Natl Acad Sci U S A. 2009; 106:16633–16638. [PubMed: 19805349]
10. Suppmann B, Sawers G. Isolation and characterization of hypophosphite--resistant mutants of *Escherichia coli*: identification of the FocA protein, encoded by the pfl operon, as a putative formate transporter. Mol Microbiol. 1994; 11:965–982. [PubMed: 8022272]
11. Waight AB, Love J, Wang DN. Structure and mechanism of a pentameric formate channel. Nature structural & molecular biology. 2010; 17:31–37.
12. Jia W, Tovell N, Clegg S, Trimmer M, Cole J. A single channel for nitrate uptake, nitrite export and nitrite uptake by *Escherichia coli* NarU and a role for NirC in nitrite export and uptake. Biochem J. 2009; 417:297–304. [PubMed: 18691156]
13. Hughes MN, Centelles MN, Moore KP. Making and working with hydrogen sulfide: The chemistry and generation of hydrogen sulfide *in vitro* and its measurement *in vivo*: a review. Free Radic Biol Med. 2009; 47:1346–1353. [PubMed: 19770036]
14. Hirshfield IN, Terzulli S, O'Byrne C. Weak organic acids: a panoply of effects on bacteria. Sci Prog. 2003; 86:245–269. [PubMed: 15508892]
15. Wang Y, et al. Structure of the formate transporter FocA reveals a pentameric aquaporin-like channel. Nature. 2009; 462:467–472. [PubMed: 19940917]
16. Lu W, et al. pH-dependent gating in a FocA formate channel. Science. 2011; 332:352–354. [PubMed: 21493860]
17. Das P, Lahiri A, Chakravortty D. Novel role of the nitrite transporter NirC in *Salmonella* pathogenesis: SPI2-dependent suppression of inducible nitric oxide synthase in activated macrophages. Microbiology. 2009; 155:2476–2489. [PubMed: 19520723]
18. Crane BR, Getzoff ED. The relationship between structure and function for the sulfite reductases. Curr Opin Struct Biol. 1996; 6:744–756. [PubMed: 8994874]
19. Hallenbeck PC, Clark MA, Barrett EL. Characterization of anaerobic sulfite reduction by *Salmonella typhimurium* and purification of the anaerobically induced sulfite reductase. J Bacteriol. 1989; 171:3008–3015. [PubMed: 2656637]
20. Wilson WJ, EMB. A combination of bismuth and sodium sulphite affording an enrichment and selective medium for the typhoid-paratyphoid groups of bacteria. J Pathol Bacteriol. 1926; 29:310–311.
21. Doyle DA, et al. The structure of the potassium channel: molecular basis of K^+ conduction and selectivity. Science. 1998; 280:69–77. [PubMed: 9525859]
22. Middleton RE, Pheasant DJ, Miller C. Purification, reconstitution, and subunit composition of a voltage-gated chloride channel from *Torpedo electroplax*. Biochemistry. 1994; 33:13189–13198. [PubMed: 7947726]
23. Savage DF, O'Connell JD 3rd, Miercke LJ, Finer-Moore J, Stroud RM. Structural context shapes the aquaporin selectivity filter. Proc Natl Acad Sci U S A. 2010; 107:17164–17169. [PubMed: 20855585]
24. Feth S, Gibbs GV, Boisen MB Jr, Myers RH. Promolecule radii for nitrides, oxides, and sulfides. A comparison with effective ionic and crystal radii. J Phys Chem. 1993; 97:11445–11450.
25. Tai CH, et al. Characterization of the allosteric anion-binding site of O-acetylserine sulfhydrylase. Biochemistry. 2001; 40:7446–7452. [PubMed: 11412097]
26. Hille, B. Ionic Channels of Excitable Membranes. Sinauer; Sunderland: 1992.
27. Yasui M, et al. Rapid gating and anion permeability of an intracellular aquaporin. Nature. 1999; 402:184–187. [PubMed: 10647010]
28. Rychkov GY, Pusch M, Roberts ML, Jentsch TJ, Bretag AH. Permeation and block of the skeletal muscle chloride channel, ClC-1, by foreign anions. J Gen Physiol. 1998; 111:653–665. [PubMed: 9565403]
29. Simons J, Jordan KD. Ab initio electronic structure of anions. Chem Rev. 1987; 87:535–555.
30. Penel S, et al. Databases of homologous gene families for comparative genomics. BMC Bioinformatics. 2009; 10 (Suppl 6):S3. [PubMed: 19534752]

31. Clamp M, Cuff J, Searle SM, Barton GJ. The Jalview Java alignment editor. Bioinformatics. 2004; 20:426–427. [PubMed: 14960472]
32. Han MV, Zmasek CM. phyloXML: XML for evolutionary biology and comparative genomics. BMC Bioinformatics. 2009; 10:356. [PubMed: 19860910]
33. Benson DA, Karsch-Mizrachi I, Lipman DJ, Ostell J, Sayers EW. GenBank. Nucleic Acids Res. 2011; 39:D32–37. [PubMed: 21071399]
34. Auer M, et al. High-yield expression and functional analysis of *Escherichia coli* glycerol-3-phosphate transporter. Biochemistry. 2001; 40:6628–6635. [PubMed: 11380257]
35. Wang DN, et al. Practical aspects of overexpressing bacterial secondary membrane transporters for structural studies. Biochim Biophys Acta. 2003; 1610:23–36. [PubMed: 12586376]
36. Cadene M, Chait B. A robust, detergent friendly method for mass spectrometry analysis of integral membrane proteins. Anal Chem. 2000; 72:5655–5658. [PubMed: 11101244]
37. Li XD, et al. Monomeric state and ligand binding of recombinant GABA transporter from *Escherichia coli*. FEBS Lett. 2001; 494:165–169. [PubMed: 11311234]
38. Safferling M, et al. The TetL tetracycline efflux protein from *Bacillus subtilis* is a dimer in the membrane and in detergent solution. Biochemistry. 2003; 42:13969–13976. [PubMed: 14636065]
39. Otwinowski Z, Miror W. Processing of X-ray diffraction data collected in oscillation mode. Meth Enzym. 1997; 276(Part A):307–326.
40. Adams PD, et al. PHENIX: building new software for automated crystallographic structure determination. Acta Crystallogr D Biol Crystallogr. 2002; 58:1948–1954. [PubMed: 12393927]
41. Emsley P, Cowtan K. Coot: model-building tools for molecular graphics. Acta Crystallogr D Biol Crystallogr. 2004; 60:2126–2132. [PubMed: 15572765]
42. Smart OS, Neduvelil JG, Wang X, Wallace BA, Sansom MS. HOLE: a program for the analysis of the pore dimensions of ion channel structural models. J Mol Graph. 1996; 14:354–360. 376. [PubMed: 9195488]
43. DeLano, WL. The PyMOL User's Manual. DeLano Scientific; San Carlos, CA: 2002.

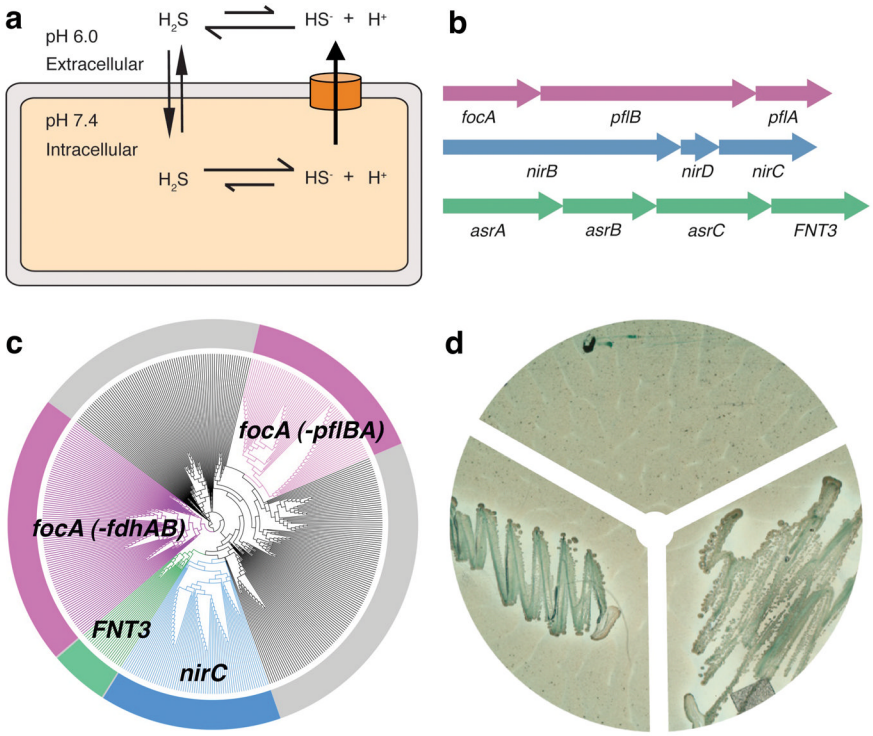

Fig. 1.

Genetic analyses and functional characterization of the *FNT3/HSC* gene and the *asrABC* operon. **a**, Model of the intracellular anion concentrative effect for the weak acid H_2S. **b**, Genomic organization of *FNT* and their metabolically related reductase genes. Representatives are shown for the *focA*, *nirC* and *FNT3/HSC* genes with their respectively linked operons. **c**, Phylogentic tree of 474 bacterial and archaeal members of the FNT family. Branches are colorized based on genetic linkage to metabolic enzymes: pyruvate formate lyase (*pflAB*) or formate dehydrogenase (*fdhAB*) linked genes are colored pink, nitrite reductase (*nirBD*) linked genes are colored blue, and sulfite reductase linked genes (*asrABC*) are colored green. The FocA protein in archaea is encoded by the *fdhC* gene. The gray areas represent FNT family members with no assigned function based on genetic linkage. **d**, Bismuth sulfite agar plate assay. *Top*: vector control, *left: asrA, asrB, asrC*, right: *asrA, asrB, asrC, FNT3.*

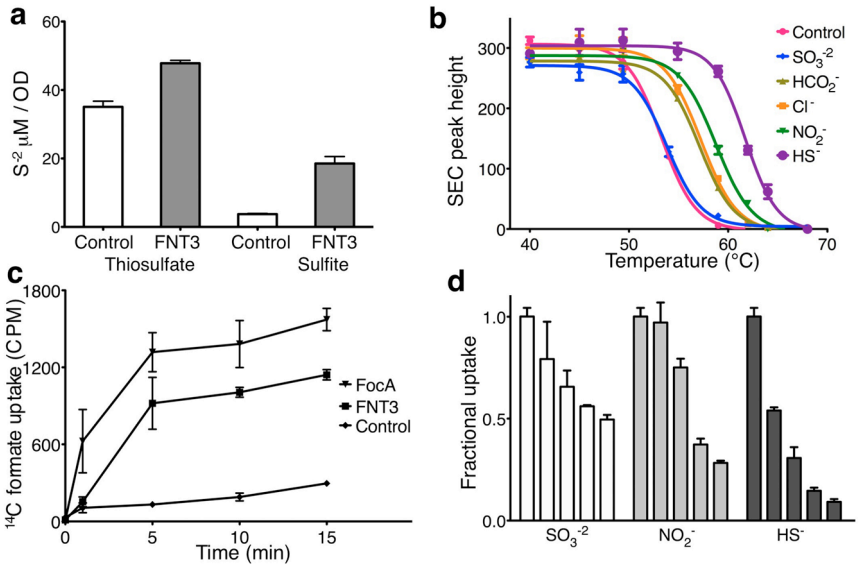

Fig 2.

Binding and transport activity of HSC channel in reconstituted proteoliposomes. **a**, Measurements of sulfide concentrations in the media of salmonella transformed with vector control or vector encoding FNT3. Minimal media was supplemented with either sulfite or thiosulfate to induce hydrogen sulfide production from either periplasmic thiosulfate reductase or cytoplasmic sulfite reductase. **b**, Binding of detergent solubilized and purified HSC protein to various anions was determined by using thermostability coupled size exclusion chromatography. Peak heights of recovered samples were plotted against temperature and fitted to a boltzman-sigmoidal model to determine nominal melting temperatures. **c**, Radiolabeled formate uptake in proteoliposomes reconstituted with purified FNT at pH 8.0 was monitored in a concentrative uptake assay and compared to FocA activity or vesicle controls. **d**, Inhibition of radiolabeled concentrative uptake of formate by the addition of various anions at increasing concentrations. The plotted bar graphs represent the amount of radiolabeled formate measured at the 10-minute time point for each concentration of anion tested. The concentration of the competing anions were, 0 mM, 0.15 mM, 0.6 mM, 3 mM and 15 mM. Error bars represent s.e.m. ($N = 3$).

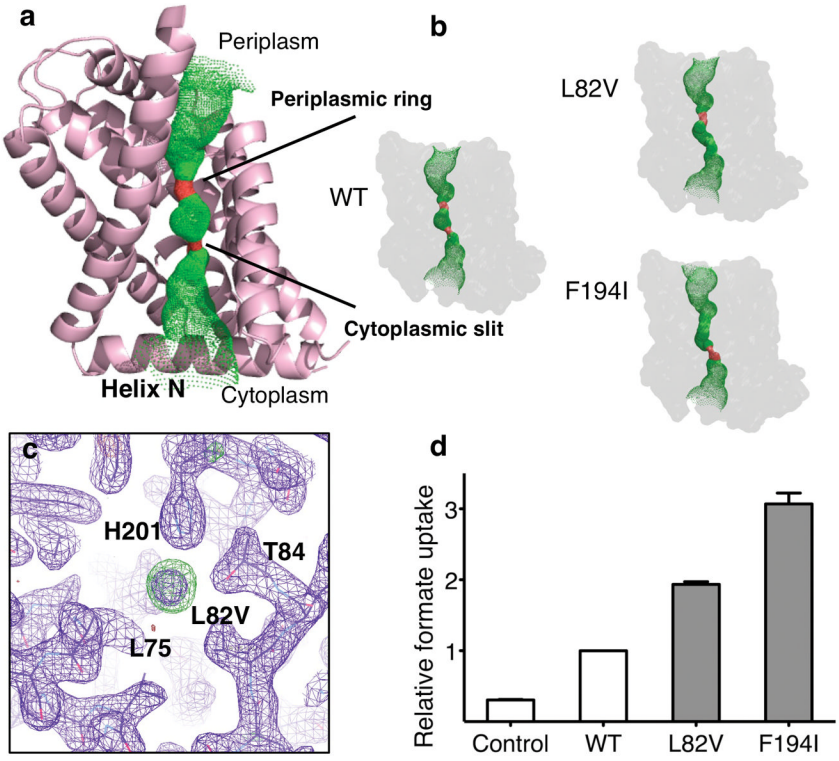

Fig 3.

Structural and functional characterization of the ion permeation pathway. **a**, Structure of a protomer of HSC overlaid with the pore diameter calculations from HOLE, colorized to indicate the radius of water, where green is permeable to water and red is impermeable. Transmembrane helix-2 has been removed for clarity. **b**, Pore diameter calculations from HOLE of the crystal structures for each of the two permeation pathway mutations, Leu82Val and Phe194Ile and wild-type (WT). **c**, Close up of the electron density observed at the selectivity filter for the Leu82Val mutant. Purple is the $2F_o - F_c$ electron density map contoured at 1.1σ and green is the $F_o - F_c$ difference density map contoured at 3σ. **d**, Relative uptake of proteoliposomes reconstituted with purified HSC protein and pathway mutations. The bar graph represents the 10-minute time point of each concentrative uptake experiment. Error bars represent s.e.m. ($N = 3$).

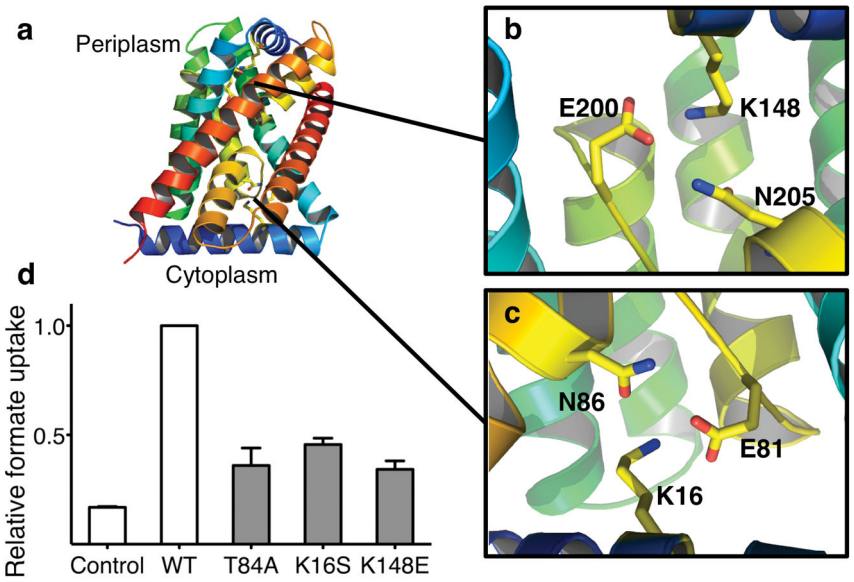

Fig 4.

Structural and functional characterization of possible gating mechanisms. **a**, Structure of the HSC protomer representing possible gating regions. The structure is colorized to show the two-fold inverted topology. **b**&**c**, The Glu-Lys-Asn salt bridge triads, related by a pseudo-twofold symmetry, help to stabilize the helix-P at the periplasmic side and helix-N at the cytoplasmic side of the protein. The rotamer that each residue adopts is conserved. **d**, Relative uptake of proteoliposomes reconstituted with purified HSC protein and gating mutations. The bar graph represents the 10-minute time point of each concentrative uptake experiment. Error bars represent s.e.m. ($N = 3$).